Analysis of Triggered Self-Excitation in Induction Generators and Experimental Validation

Marc Bodson, *Fellow, IEEE,* and Oleh Kiselychnyk

***Abstract*—In self-excited induction machines, a power generating mode of operation can often be attained only by pre-charging at least one of the capacitors connected to the windings. The paper shows how a carefully derived state-space model with nonlinear magnetic characteristics enables the assessment of all possible operating regimes including their stability properties. In particular, the analysis reveals the possible existence of an unstable operating regime, which creates a barrier that must be overcome through pre-charged capacitors. In such case, the analytical results of the paper yield a simple formula that predicts the voltage needed to trigger self-excitation. Close to the boundary, voltages can be generated for extended periods of time before growing to a stable operating regime, or collapsing to zero. Experimental results validate the results of the paper on the transient properties of self-excited induction generators.**

***Index Terms*—induction generator, self-excitation, nonlinear dynamic model, renewable energy, electric machines.**

I. Introduction

Induction generators have found applications in renewable energy (wind and hydro), due to their ability to generate electric power at frequencies that are not exactly tied to their frequency of rotation. Although wound-rotor induction machines are often used, squirrel-cage generators have significant benefits in terms of cost and robustness. They can generate power off-grid as self-excited induction generators (SEIG's), with capacitors placed in parallel with the loads.

Steady-state operation of the SEIG can be analyzed using the steady-state equivalent circuit of the induction generator, where the total loop impedance [1]-[4] or the total node admittance at the magnetizing branch [5]-[7] is equated to zero. Such condition is necessary because the zero state is always a possible steady-state of the system, and power generation is only possible if another, non-zero periodic steady-state exists in the nonlinear magnetic saturation region.

The transient response of the SEIG is more complicated to analyze. A standard approach uses the generalized model of the induction machine [8]-[11] to search for parameters such that the system of differential equations describing the SEIG becomes unstable around the zero state. We refer to this condition as *spontaneous self-excitation*. In this case, the generator voltages diverge from the zero state exponentially, starting from arbitrarily small initial conditions, and converge to sinusoidal voltages with magnitude and frequency depending on the system parameters. Analytic conditions replacing the extensive numerical computations of the eigenvalues of the 6x6 matrix associated with the linearized model of the SEIG were derived in [12].

Experiments, however, show that a non-zero operating regime can exist even when the zero state is stable and is often the most common mode of operation of the SEIG. In this case, the induction generator needs to be "kicked" in order to transfer operation to the non-zero steady-state. Typically, this is achieved by starting the machine with pre-charged capacitors at sufficiently high voltages, a condition that we refer to as *triggered self-excitation*.

The available theory of self-excitation leaves open many questions related to triggered self-excitation. In particular, how many steady-states are possible? How does one know whether a computed steady-state is stable? How does one explain the need for pre-charged capacitors, or compute the capacitor voltage needed to trigger self-excitation?

To provide answers to these questions, the paper starts by developing a state-space model of the induction generator with nonlinear magnetic characteristics. Consistent with some of the research on SEIG [13]-[15], the model takes into account the non-linearity of the magnetizing inductance not only in the high current region (magnetic saturation), but also in the low current region. As opposed to many studies of the SEIG which only incorporate magnetic nonlinearities in the steady-state model, the paper carefully integrates the nonlinearity in the state-space model using the approach of [16], [17]. This approach enables the analysis of the stability properties of the operating points. In particular, it is found that a non-zero, unstable operating steady-state of the SEIG is possible. The unstable steady-state creates the barrier that must be overcome by triggered self-excitation. With this understanding, the paper shows that it is possible to compute simply and precisely the value of the capacitor voltage required.

The paper includes results presented in conferences [12][15][18][19], while providing a unified and concise presentation of the new contributions to the theory of self-excited induction generators. For clarity of presentation, all the theoretical results are first presented, and are then followed by the experimental results validating the analysis and illustrating interesting characteristics of the SEIG. Contributions of the paper include an analysis of the number of possible operating steady-states and of their stability, a justification of the

Manuscript received March 18, 2011.

This work was supported in part by the U.S. Department of State under Fulbright Grant 68431809.

M. Bodson is with the ECE Department, University of Utah, Salt Lake City, UT 84112, USA (e-mail: bodson@eng.utah.edu)

O. Kiselychnyk is with the FEA Faculty, National Technical University of Ukraine "Kiev Polytechnic Institute", Kiev, Ukraine, 03056, (e-mail: koi@gala.net)

possible need for triggered self-excitation based on the existence of an unstable operating steady-state, an explicit formula predicting the continuous dependency of the minimum speed on the initial capacitor voltage, and an explanation of the slow growth/collapse of voltages observed under certain conditions.

II. Analytical Results

A. Mathematical Model of an Induction Generator

The standard model of a two-phase induction generator in an arbitrary coordinate frame consists of the vector differential equations

$$\frac{d\Psi_S}{dt} = U_S - R_S i_S - \omega_e J \Psi_S, \quad J = \begin{bmatrix} 0 & -1 \\ 1 & 0 \end{bmatrix},$$

$$\frac{d\Psi_R}{dt} = -R_R i_R + (n_p\omega - \omega_e) J \Psi_R, \tag{1}$$

where $\Psi_S = [\Psi_{SF} \ \Psi_{SG}]^T$, $\Psi_R = [\Psi_{RF} \ \Psi_{RG}]^T$ are vectors of stator and rotor total flux linkages, $i_S = [i_{SF} \ i_{SG}]^T$, $i_R = [i_{RF} \ i_{RG}]^T$ are vectors of stator and rotor currents, $U_S = [U_{SF} \ U_{SG}]^T$ is a vector of stator voltages, R_S and R_R are the stator and rotor resistances, n_p is the number of pole pairs, ω is the angular velocity of the rotor, and ω_e is the angular velocity of the arbitrary coordinate frame. Resistive loads are connected in parallel with capacitors to the stator windings, resulting in the additional vector equation

$$-C\frac{dU_S}{dt} = i_S + Y_L U_S + \omega_e C J U_S, \tag{2}$$

where Y_L is the admittance of the resistive load and C is the value of the capacitor (both added to each phase).

The F and G indices denote the components associated with the rotating coordinate frame. For the stator currents,

$$\begin{pmatrix} i_{SF} \\ i_{SG} \end{pmatrix} = \begin{pmatrix} \cos(\theta_e) & \sin(\theta_e) \\ -\sin(\theta_e) & \cos(\theta_e) \end{pmatrix} \begin{pmatrix} i_{SA} \\ i_{SB} \end{pmatrix}, \tag{3}$$

where i_{SA}, i_{SB} are the currents in the windings A and B and θ_e is the angle of the coordinate frame with respect to the A winding. A similar expression applies for the voltages. For the rotor variables, θ_e is replaced by $\theta_e - n_P\,\theta$, where θ is the angular position of the rotor. The angular velocities are given by $\omega_e = d\theta_e/dt$ and $\omega = d\theta/dt$. In the case of a three-phase generator, a three-phase to two-phase transformation should be used to apply the results.

The magnetizing current of the induction generator is the sum of the stator current and the rotor current. The amplitude of the magnetizing current is

$$i_M = \sqrt{i_{MF}^{\,2} + i_{MG}^{\,2}}, \ i_{MF} = i_{SF} + i_{RF}, \ i_{MG} = i_{SG} + i_{RG}. \tag{4}$$

Following the approach of [16], [17], the stator and rotor flux linkages are assumed to be of the form

$$\Psi_S = L_{\sigma S} i_S + L_M (i_S + i_R), \ \Psi_R = L_{\sigma R} i_R + L_M (i_S + i_R), \tag{5}$$

where $L_{\sigma S}$ and $L_{\sigma R}$ are the stator and rotor leakage inductances, and L_M is the stator-rotor mutual inductance, also called *magnetizing inductance*. Saturation of the leakage inductances is neglected on the basis that they constitute a small fraction of the overall inductances, and the magnetizing inductance is solely considered a nonlinear function of the magnetizing current with

$$L_M = \Psi_M / i_M, \tag{6}$$

where Ψ_M denotes the amplitude of the main magnetic flux linkage. We have

$$\frac{dL_M}{di_M} = \frac{d(\Psi_M / i_M)}{di_M} = \frac{L - L_M}{i_M}, \tag{7}$$

where we defined

$$L = d\Psi_M / di_M = L_M + i_M dL_M / di_M, \tag{8}$$

as the *dynamic magnetizing inductance*. The magnetizing inductance and the dynamic magnetizing inductance are equal for a linear magnetic circuit, but not otherwise.

The time-derivative of the magnetizing current amplitude is

$$\frac{di_M}{dt} = \frac{1}{2i_M}\frac{d(i_{MF}^2 + i_{MG}^2)}{dt} = \frac{i_{MF}}{i_M}\frac{di_{MF}}{dt} + \frac{i_{MG}}{i_M}\frac{di_{MG}}{dt}, \tag{9}$$

so that the time-derivative of the magnetizing inductance becomes

$$\frac{dL_M}{dt} = \frac{dL_M}{di_M}\frac{di_M}{dt} = \frac{(L - L_M)}{i_M^2}\left(i_{MF}\frac{di_{MF}}{dt} + i_{MG}\frac{di_{MG}}{dt}\right). \tag{10}$$

Using these expressions in the time-derivatives of the stator and rotor flux linkages, one obtains

$$\frac{d\Psi_S}{dt} = (L_{\sigma S} + L_M)\frac{di_S}{dt} + L_M\frac{di_R}{dt} + \frac{dL_M}{dt}(i_S + i_R),$$

$$\frac{d\Psi_R}{dt} = (L_{\sigma R} + L_M)\frac{di_R}{dt} + L_M\frac{di_S}{dt} + \frac{dL_M}{dt}(i_S + i_R), \tag{11}$$

and then, the model of the induction generator in the form of the implicit nonlinear differential matrix equation

$$E\dot{X} = FX, \tag{12}$$

where

$$E = \begin{bmatrix} -C & 0 & 0 & 0 & 0 & 0 \\ 0 & L_{\sigma S} + L_{MF} & L_{MF} & 0 & L_{MFG} & L_{MFG} \\ 0 & L_{MF} & L_{\sigma R} + L_{MF} & 0 & L_{MFG} & L_{MFG} \\ 0 & 0 & 0 & -C & 0 & 0 \\ 0 & L_{MFG} & L_{MFG} & 0 & L_{\sigma S} + L_{MG} & L_{MG} \\ 0 & L_{MFG} & L_{MFG} & 0 & L_{MG} & L_{\sigma R} + L_{MG} \end{bmatrix},$$

$$F = \begin{bmatrix} Y_L & 1 & 0 \\ 1 & -R_S & 0 \\ 0 & 0 & -R_R \\ C\omega_e & 0 & 0 \\ 0 & -\omega_e(L_{\sigma S} + L_M) & -\omega_e L_M \\ 0 & (n_p\omega - \omega_e)L_M & (n_p\omega - \omega_e)(L_{\sigma R} + L_M) \end{bmatrix}$$

$$\begin{bmatrix} -C\omega_e & 0 & 0 \\ 0 & \omega_e(L_{\sigma S} + L_M) & \omega_e L_M \\ 0 & (\omega_e - n_p\omega)L_M & (\omega_e - n_p\omega)(L_{\sigma R} + L_M) \\ Y_L & 1 & 0 \\ 1 & -R_S & 0 \\ 0 & 0 & -R_R \end{bmatrix},$$

$$X = [U_{SF} \ i_{SF} \ i_{RF} \ U_{SG} \ i_{SG} \ i_{RG}]^T, \tag{13}$$

and

$$L_{MF} = L_M + (L - L_M) i_{MF}^2 / i_M^2 \,,\; L_{MG} = L_M + (L - L_M) i_{MG}^2 / i_M^2 \,,$$
$$L_{MFG} = (L - L_M) i_{MF} i_{MG} / i_M^2 \,. \tag{14}$$

Note that E and F are nonlinear functions of X through L_M, L_{MF}, L_{MG}, and L_{MFG}. Equation (12) can be transformed into the standard explicit form

$$\dot{X} = AX \,, \tag{15}$$

by defining $A = E^{-1}F$. In this form, standard numerical integration methods can be used. However, the system remains a nonlinear system, since A is a function of X.

An interesting alternative representation of the model can be obtained by using the following equalities

$$(L_{MF} - L_M)\left(\frac{di_{SF}}{dt} + \frac{di_{RF}}{dt}\right) + L_{MFG}\left(\frac{di_{SG}}{dt} + \frac{di_{RG}}{dt}\right) = (L - L_M)\frac{i_{MF}}{i_M}\frac{di_M}{dt} \,, \tag{16}$$

$$(L_{MG} - L_M)\left(\frac{di_{SG}}{dt} + \frac{di_{RG}}{dt}\right) + L_{MFG}\left(\frac{di_{SF}}{dt} + \frac{di_{RF}}{dt}\right) = (L - L_M)\frac{i_{MG}}{i_M}\frac{di_M}{dt} \,. \tag{17}$$

Substituting (16) and (17) into (12) and (13) gives the matrix equation

$$E_L \dot{X} = FX - \frac{L - L_M}{i_M}\frac{di_M}{dt} X_M \,, \tag{18}$$

where $X_M = [0\; i_{MF}\; i_{MF}\; 0\; i_{MG}\; i_{MG}]^T$ and

$$E_L = \begin{bmatrix} -C & 0 & 0 & 0 & 0 & 0 \\ 0 & L_{\sigma S} + L_M & L_M & 0 & 0 & 0 \\ 0 & L_M & L_{\sigma R} + L_M & 0 & 0 & 0 \\ 0 & 0 & 0 & -C & 0 & 0 \\ 0 & 0 & 0 & 0 & L_{\sigma S} + L_M & L_M \\ 0 & 0 & 0 & 0 & L_M & L_{\sigma R} + L_M \end{bmatrix}. \tag{19}$$

Note that

$$E_L \dot{X} = FX \tag{20}$$

is the model of the induction generator with linear magnetics, which is indeed verified since $L = L_M$ in that case. However, the second term of (18) also drops out if di_M/dt=0. In other words, if a solution of (20) is obtained for which the magnetizing current is constant, it is also a solution of the nonlinear system (18). This justifies the use of the linear model (19)-(20) with L_M a function of i_M to obtain steady-state responses, but one should remember that the general dynamic model is more complicated.

B. Determination of Possible Operating Modes

The determination of an operating mode can be performed by finding a periodic steady-state solution to the induction generator model in the stator frame of reference (ω_e=0). Alternatively, one can use the (equivalent) approach that consists in finding a frequency ω_e^* such that a *constant* solution exists in a rotating frame of reference. With either (12) or (18), the condition for such a constant solution is that there exists a vector X^* such that

$$F^* X^* = 0 \,, \tag{21}$$

where F^* is the function F evaluated at the equilibrium X^* and at the frequency ω_e^* to be determined. The matrix F^* has the special structure

$$F^* = \begin{bmatrix} F_1^* & -F_2^* \\ F_2^* & F_1^* \end{bmatrix}, \tag{22}$$

so that, for X^* partitioned similarly as $X^* = \begin{bmatrix} X_1^* & X_2^* \end{bmatrix}^T$, equation (21) becomes

$$F_1^* X_1^* - F_2^* X_2^* = 0,\; F_2^* X_1^* + F_1^* X_2^* = 0. \tag{23}$$

The existence of a nonzero vector X^* such that (21) is satisfied is thus equivalent to the existence of a nonzero complex vector $Z^* = X_1^* + jX_2^*$ such that

$$\left(F_1^* + jF_2^*\right) Z^* = 0 \,, \tag{24}$$

which occurs if and only if $\det(F_1^* + jF_2^*) = 0$. Using (13),

$$F_1^* + jF_2^* = \begin{bmatrix} Y_L + jC\omega_e^* & 1 & 0 \\ 1 & -R_S - j\omega_e^*(L_{\sigma S} + L_M^*) & -j\omega_e^* L_M^* \\ 0 & j\left(n_p\omega - \omega_e^*\right)L_M^* & -R_R + j\left(n_p\omega - \omega_e^*\right)(L_{\sigma R} + L_M^*) \end{bmatrix}, \tag{25}$$

so that the real and imaginary parts of $\det(F_1^* + jF_2^*) = 0$ are equal to

$$\begin{aligned} \mathrm{Re}\left(\det\left(F_1^* + jF_2^*\right)\right) &= c_1 L_M^* + c_2 = 0, \\ \mathrm{Im}\left(\det\left(F_1^* + jF_2^*\right)\right) &= c_3 L_M^* + c_4 = 0, \end{aligned} \tag{26}$$

where c_1, c_2, c_3 and c_4 are given by

$$\begin{aligned} c_1 &= -\omega_e^{*2} C R_R - \omega_e^*\left(\omega_e^* - n_p\omega\right)\left(Y_L L_{\sigma S} + Y_L L_{\sigma R} + CR_S\right), \\ c_2 &= R_R\left(1 + Y_L R_S\right) - \omega_e^{*2} C R_R L_{\sigma S} \\ &\quad - \omega_e^*\left(\omega_e^* - n_p\omega\right) L_{\sigma R}\left(Y_L L_{\sigma S} + CR_S\right), \\ c_3 &= \omega_e^* Y_L R_R - \left(\omega_e^* - n_p\omega\right)\left(\omega_e^{*2} C\left(L_{\sigma S} + L_{\sigma R}\right) - Y_L R_S - 1\right), \\ c_4 &= \omega_e^* C R_S R_R + \omega_e^* Y_L R_R L_{\sigma S} \\ &\quad - \left(\omega_e^* - n_p\omega\right)\left(\omega_e^{*2} C L_{\sigma S} L_{\sigma R} - Y_L R_S L_{\sigma R} - L_{\sigma R}\right). \end{aligned} \tag{27}$$

The two unknowns that must be determined using the two conditions in (26) are the frequency ω_e^* and the magnetizing inductance L_M^* (which, in turn, gives the magnetizing current i_M^* corresponding to the steady-state). One way to solve the equations is to eliminate L_M^* from (26), which results in a 5th order polynomial equation in ω_e^*

$$
\begin{aligned}
&C^2\left(R_S L_{\sigma R}^2 + R_R L_{\sigma S}^2\right)\omega_e^{*5} - n_p\omega C^2\left(2R_S L_{\sigma R}^2 + R_R L_{\sigma S}^2\right)\omega_e^{*4} \\
&+\left(\left(n_p\omega\right)^2 C^2 R_S L_{\sigma R}^2 + C^2 R_R^2 R_S + C^2 R_R R_S^2 - 2CR_R L_{\sigma S}\right. \\
&\left.+Y_L^2 R_S L_{\sigma R}^2 + Y_L L_{\sigma R}^2 + Y_L^2 R_R L_{\sigma S}^2\right)\omega_e^{*3} - n_p\omega\left(C^2 R_R R_S^2\right. \\
&\left.-2CR_R L_{\sigma S} + 2Y_L^2 R_S L_{\sigma R}^2 + 2Y_L L_{\sigma R}^2 + Y_L^2 R_R L_{\sigma S}^2\right)\omega_e^{*2} \\
&+\left(Y_L R_S + 1\right)\left(R_R + Y_L R_R^2 + \left(n_p\omega\right)^2 L_{\sigma R}^2 Y_L + Y_L R_S R_R\right)\omega_e^{*} \\
&-n_p\omega R_R\left(Y_L R_S + 1\right)^2 = 0.
\end{aligned}
\tag{28}
$$

Although up to five solutions are possible, computations with realistic motor parameters typically yield at most one real positive solution ω_e^*. Substitution of ω_e^* in either equation of (26) then gives L_M^*. One or more values of i_M^* may be possible for a given L_M^*, depending on the shape of the magnetizing curve.

It remains to characterize the solutions in terms of X^*, so that stability of the equilibrium points can be assessed. With $U_S^* = U_{SF}^* + jU_{SG}^*$, $i_S^* = i_{SF}^* + ji_{SG}^*$, $i_R^* = i_{RF}^* + ji_{RG}^*$, and $Z^* = \left[U_S^*, i_S^*, i_R^*\right]^T$, the first two rows of (24)-(25) give

$$
\begin{aligned}
i_S^* &= -\left(Y_L + jC\omega_e^*\right)U_S^*, \\
i_R^* &= \frac{\left(1+\left(Y_L + jC\omega_e^*\right)\left(R_S + j\omega_e^*(L_{\sigma S} + L_M^*)\right)\right)}{j\omega_e^* L_M^*}U_S^*.
\end{aligned}
\tag{29}
$$

The third row of (24) is linearly dependent on the first two rows, due to $\det(F_1^* + jF_2^*) = 0$, and does not give any additional condition. On the other hand, the fact that $i_M^* = \left|i_S^* + i_R^*\right|$ implies, using (29), that

$$
\left|U_S^*\right| = \frac{\omega_e^* L_M^* i_M^*}{\sqrt{(1+Y_L R_S - C\omega_e^{*2} L_{\sigma s})^2 + \omega_e^{*2}(Y_L L_{\sigma s} + CR_S)^2}}. \tag{30}
$$

An equilibrium vector X^* is characterized by a voltage U_S^* of arbitrary angle and magnitude given by (30), and currents i_S^*, i_R^* given by (29). There are an infinite number of equilibrium states, which are all identical except for a shift in angle of the generated voltages and currents (the relative phases remain the same).

C. Stability of Operating Modes

It would be tempting to assume that the stability of the system linearized around an equilibrium point X^* is determined by the eigenvalues of the matrix $A^*=(E^*)^{-1}F^*$. However, this is not correct if $X^* \neq 0$. The stability of the nonlinear system in the vicinity of X^* can be determined by considering small perturbations δX with $X = X^* + \delta X$. For such perturbations around the equilibrium, a first-order description is

$$
\begin{aligned}
&\left(E^* + \left[\frac{\partial E}{\partial X}\right]^* \delta X\right)\left(\dot{X}^* + \delta\dot{X}\right) \\
&= \left(F^* + \left[\frac{\partial F}{\partial X}\right]^* \delta X\right)\left(X^* + \delta X\right),
\end{aligned}
\tag{31}
$$

where E^* and F^* are the values of the matrices E and F at the equilibrium and

$$
\left[\frac{\partial E}{\partial X}\right]^* \delta X = \sum_{k=1}^{n}\left[\frac{\partial E}{\partial X_k}\right]^* \delta X_k \,. \tag{32}
$$

The term in the second bracket is the matrix obtained by taking the partial derivative of the matrix E with respect to the k^{th} element of X and evaluating the elements of the resulting matrix at the equilibrium values. The summation is performed over the n elements of δX. A similar definition applies for F.

Using the fact that $\dot{X}^* = 0$ and $F^* X^* = 0$, and neglecting second-order terms, one obtains the linearized description of the system around the equilibrium

$$
E^*\delta\dot{X} = F^*\delta X + \left[\frac{\partial F}{\partial X}\right]^* \delta X\, X^* . \tag{33}
$$

Equation (33) can be put in the form

$$
E^*\delta\dot{X} = \left(F^* + \delta F^*\right)\delta X, \tag{34}
$$

where the $(i,j)^{th}$ element of the matrix δF^* is given by

$$
\delta F_{ij}^* = \sum_{k=1}^{n}\left[\frac{\partial F_{ik}}{\partial X_j}\right]^* X_k^* . \tag{35}
$$

Thus, the equilibrium vector X^* is stable if and only if all the eigenvalues of the matrix

$$
A^* = \left(E^*\right)^{-1}\left(F^* + \delta F^*\right) \tag{36}
$$

are in the open left-half plane.

For the induction generator, E^* and F^* are obtained by replacing the inductances L_M, L_{MF}, L_{MG}, and L_{MFG} in (13) by the equilibrium values and by replacing ω_e by ω_e^*. δF^* is given by

$$
\delta F^* = \begin{bmatrix}
0 & 0 & 0 \\
0 & \omega_e^*\delta_5 & \omega_e^*\delta_6 \\
0 & (\omega_e^* - n_p\omega)\delta_5 & (\omega_e^* - n_p\omega)\delta_6 \\
0 & 0 & 0 \\
0 & -\omega_e^*\delta_1 & -\omega_e^*\delta_2 \\
0 & (n_p\omega - \omega_e^*)\delta_1 & (n_p\omega - \omega_e^*)\delta_2
\end{bmatrix}
\begin{bmatrix}
0 & 0 & 0 \\
0 & \omega_e^*\delta_3 & \omega_e^*\delta_4 \\
0 & (\omega_e^* - n_p\omega)\delta_3 & (\omega_e^* - n_p\omega)\delta_4 \\
0 & 0 & 0 \\
0 & -\omega_e^*\delta_7 & -\omega_e^*\delta_8 \\
0 & (n_p\omega - \omega_e^*)\delta_7 & (n_p\omega - \omega_e^*)\delta_8
\end{bmatrix}, \tag{37}
$$

where

$$
\delta_1 = \left(\frac{\partial L_M}{\partial i_{SF}}\right)^* i_{MF}^*,\ \delta_2 = \left(\frac{\partial L_M}{\partial i_{RF}}\right)^* i_{MF}^*,\ \delta_3 = \left(\frac{\partial L_M}{\partial i_{SG}}\right)^* i_{MG}^*,
$$

$$
\delta_4 = \left(\frac{\partial L_M}{\partial i_{RG}}\right)^* i_{MG}^*,\ \delta_5 = \left(\frac{\partial L_M}{\partial i_{SF}}\right)^* i_{MG}^*,\ \delta_6 = \left(\frac{\partial L_M}{\partial i_{RF}}\right)^* i_{MG}^*,
$$

$$\delta_7 = \left(\frac{\partial L_M}{\partial i_{SG}}\right)^* i^*_{MF},\ \delta_8 = \left(\frac{\partial L_M}{\partial i_{RG}}\right)^* i^*_{MF}. \quad (38)$$

The terms in parentheses can be determined using

$$\left(\frac{\partial L_M}{\partial i_{SF}}\right)^* = \left(\frac{dL_M}{di_M}\right)^* \left(\frac{\partial i_M}{\partial i_{SF}}\right)^* = \left(\frac{\partial L_M}{\partial i_{RF}}\right)^* = \frac{L^* - L^*_M}{i^*_M}\frac{i^*_{MF}}{i^*_M}, \quad (39)$$

and similarly for i_{SG}, i_{RG}.

Note that an arbitrary equilibrium vector can be transformed through a shift of angle in the *FG* reference frame into an equilibrium vector with $i^*_{MF} = i^*_M$, $i^*_{MG} = 0$. In this case, E^* and F^* are obtained by setting $L^*_{MF} = L^*$, $L^*_{MG} = L^*_M$, $L^*_{MFG} = 0$ while, in (37),

$$\delta_1 = \delta_2 = L^* - L^*_M,\ \delta_3 = \delta_4 = \delta_5 = \delta_6 = \delta_7 = \delta_8 = 0. \quad (40)$$

Because all the equilibrium vectors X^* associated with some ω^*_e and i^*_M can be transformed into the same equilibrium vector by a rotation of the reference axes, the systems linearized around all equilibrium vectors must have the same eigenvalues. For this reason, we will talk about "the" equilibrium state associated with a given ω^*_e and i^*_M, even though there are technically infinitely many (all equivalent) such equilibrium states.

D. General Characteristics of Operating Modes

Fig. 1 shows the general shape of a magnetizing inductance as a function of the magnetizing current. The curve includes an ascending part rising from L_{MO} to L_{MAX}, a (more or less) flat part at L_{MAX} corresponding to a linear magnetic regime, and a descending part corresponding to magnetic saturation. Often, the ascending part of the curve is neglected (L_{MO}=L_{MAX}). However, several works [13]-[15] have shown the need to represent this nonlinearity at low currents to accurately model self-excitation in induction generators.

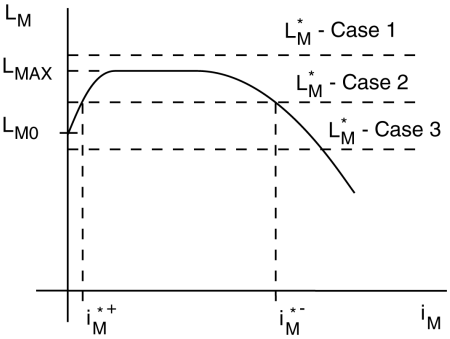

Fig. 1. Magnetization curve and three possible cases of steady-state values.

Three cases are shown on the figure:

- Case 1: with $L^*_M > L_{MAX}$, the generator has only one equilibrium state corresponding to $i^*_M = 0$.
- Case 2: with $L_{MAX} > L^*_M > L_{M0}$, the generator has three equilibrium states: $i^*_M = 0$, i^{*+}_M corresponding to the ascending part of the curve, and i^{*-}_M corresponding to the descending part of the curve.
- Case 3: with $L_{M0} > L^*_M$, the generator has two equilibrium states $i^*_M = 0$ and i^{*-}_M corresponding to the descending part of the curve.

Computations and experimental results to be presented hereafter have shown the following properties:

- Case 1: the equilibrium corresponding to $i^*_M = 0$ is stable.
- Case 2: the equilibrium corresponding to $i^*_M = 0$ and i^{*-}_M are stable. The equilibrium corresponding to i^{*+}_M is unstable.
- Case 3: the equilibrium state corresponding to $i^*_M = 0$ is unstable and the equilibrium corresponding to i^{*-}_M is stable.

In case 1, a power generating mode of self-excitation is not possible. In case 3, a power generating mode of self-excitation is possible and will naturally develop, due to the instability of the zero state. We refer to this condition as *spontaneous self-excitation*. In case 2, two power generating modes exist. The one associated with the lower magnetizing current is unstable, and cannot be sustained indefinitely (although experiments show that it may be for some extended periods of time). If the unstable state is reached, small perturbations will either make the magnetizing current grow, resulting in the equilibrium state with higher magnetizing current to be reached, or to decay, resulting in a collapse of the voltage. Since, the zero state is stable: the generator will not naturally leave this state.

Simulations and experiments have shown that, to reach the stable power generating mode, the magnetizing current must be brought to a value greater than or equal to i^{*+}_M. This condition can be achieved, for example, by applying sufficiently large initial voltages to the capacitors. We refer to this condition as *triggered self-excitation*. Sometimes, it is also possible for residual magnetization to produce the result, but it is not a triggering mechanism that one can reliably depend upon.

E. Boundaries of Self-Excitation

As Fig. 1 shows, critical changes occur when $L^*_M = L_{MAX}$ and $L^*_M = L_{M0}$. For a given L^*_M, $\omega^*_e - n_p\omega$ can be eliminated from the two equations of (26), yielding the quartic equation in ω^*_e given by

$$f_1\omega^{*4}_e + f_2\omega^{*2}_e + f_3 = 0, \quad (41)$$

where

$$f_1 = C^2 L^*_S\left(L^*_S L^*_R - L^{*2}_M\right) > 0,$$
$$f_2 = Y^2_L L^*_S\left(L^*_S L^*_R - L^{*2}_M\right) + C^2 R^2_S L^*_R - C\left(2L^*_S L^*_R - L^{*2}_M\right), \quad (42)$$
$$f_3 = L^*_R\left(Y_L R_S + 1\right)^2 > 0,$$

with $L^*_S = L_{\sigma S} + L^*_M$, $L^*_R = L_{\sigma R} + L^*_M$. The quartic equation is a quadratic equation in ω^{*2}_e, which has a real positive solution if and only if

$$f_2 < -2\sqrt{f_1 f_3}. \quad (43)$$

If (43) is satisfied, there are two real positive solutions to the quadratic equation, and we denote the two square roots of

these solutions $\omega^*_{e,\min}$ and $\omega^*_{e,\max}$. These are the solutions of the quartic equation. The velocity ω can be determined from ω^*_e using either equation of (26). Specifically, the first equation gives

$$\omega = \frac{1}{n_P}\left(\omega^*_e - \frac{Y_L R_S R_R - \omega^{*2}_e C R_R L^*_S + R_R}{\omega^*_e\left(Y_L\left(L^*_S L^*_R - L^{*2}_M\right) + R_S L^*_R C\right)}\right). \qquad (44)$$

From $\omega^*_{e,\min}$ and $\omega^*_{e,\max}$, velocities $\omega_{\min}$ and $\omega_{\max}$ can be determined in this manner. The velocities constitute the boundaries where self-excitation is possible. If the procedure is applied with $L^*_M = L_{MAX}$, the boundaries of self-excitation (which may require triggering to be reached) are obtained. If $L^*_M = L_{M0}$ is used, the boundaries of spontaneous self-excitation are obtained.

F. Triggered Self-Excitation

An unstable equilibrium state creates a barrier that can be overcome by reaching a magnetizing current greater than i^{*+}_M, the magnetizing current associated with the unstable equilibrium state. In practice, the magnetizing current cannot be directly controlled, but a sufficiently large initial capacitor voltage on one of the phases can transfer the zero state to a state with the required magnetizing current, thus triggering self-excitation. Although the exact relationship between the initial capacitor voltage and the magnetizing current depends on the highly nonlinear dynamics of the system, a simple approximation based on the linear system has been found to give surprisingly accurate results.

Specifically, Fig. 2 shows the results of a simulation of the system linearized around $X = 0$ (with the matrix $A_c(s)$ describing the system, as shown below), and with zero initial conditions, except for one of the capacitor voltages. Notice the short period of time on the time axis, which is much shorter than the time associated with the build-up or collapse of self-excitation. The response of the magnetizing current is shown for three speeds. The curve in the middle is the response at the critical speed where the system has a pole at *s=0*. Above and below are the responses at higher and lower speeds, respectively, which correspond to systems with unstable and stable poles.

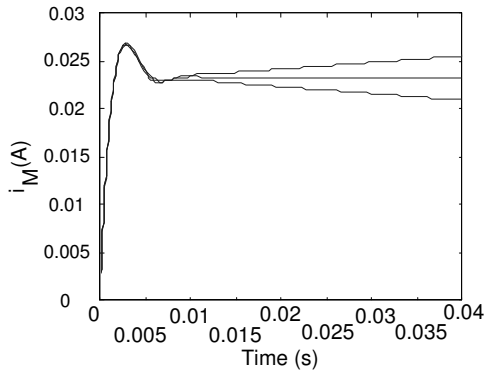

Fig. 2. Growth of the magnetizing current in three cases

As can be seen on the figure, the magnetizing current reaches a peak value at about 2.5ms and then, what we will call a *temporary steady-state value* at about 10ms. The currents i_M at 10ms are nearly identical, and the temporary steady-state value is the actual steady-state value for the system with a pole at *s=0*. Of course, the currents at the initial peak value of the response are also nearly identical, and it would be intuitive to assume that this value would be the critical factor in determining the success in triggering self-excitation. However, it was found that a more accurate predictor was whether the temporary steady-state value was greater than i^{*+}_M.

It remains to determine how the initial capacitor voltage relates to the temporary steady-state current. Linearizing the system around the zero state, $\delta F^* = 0$ and $\delta X = X$. Applying the Laplace transform, (34) becomes

$$\left(sE^* - F^*\right)X(s) = X_0, \qquad (45)$$

where, with some abuse of notation, $X(s)$ is the Laplace transform of $X(t)$ and X_0 is the initial condition of X. Analysis can be simplified by defining a complex vector

$$X_c = \begin{bmatrix} X_{c,1} \\ X_{c,2} \\ X_{c,3} \end{bmatrix} = \begin{bmatrix} U_{SF} + jU_{SG} \\ i_{SF} + ji_{SG} \\ i_{RF} + ji_{RG} \end{bmatrix}. \qquad (46)$$

Reorganizing the equations, (45) becomes

$$A_c(s)X_c(s) = \begin{bmatrix} CX_{c,1}(0) \\ 0 \\ 0 \end{bmatrix}, \qquad (47)$$

where

$$A_C(s) = \begin{bmatrix} (s + j\omega^*_e)C + Y_L & 1 & 0 \\ -1 & (s + j\omega^*_e)L_{S0} + R_S & (s + j\omega^*_e)L_{M0} \\ 0 & (s + j\omega^*_e)L_{M0} - jn_p\omega L_{M0} & (s + j\omega^*_e)L_{R0} + R_R - jn_p\omega L_{R0} \end{bmatrix},$$

and $X_{c,1}(0)$ denotes the initial value of $X_{c,1}$, while $L_{S0} = L_{M0} + L_{\sigma S}$ and $L_{R0} = L_{M0} + L_{\sigma R}$. $\left|X_{c,1}(0)\right| = U_C$, the initial voltage applied to the capacitor if only one capacitor is pre-charged (or the magnitude of the complex vector otherwise), and $i_M(t) = |X_{c,2}(t) + X_{c,3}(t)|$.

Solving the system of equations (47) gives

$$\begin{bmatrix} X_{c,2} \\ X_{c,3} \end{bmatrix} = \frac{CX_{c,1}(0)}{\det(A_C(s))}\begin{bmatrix} (s + j\omega^*_e)L_{R0} + R_R - jn_p\omega L_{R0} \\ -((s + j\omega^*_e)L_{M0} - jn_p\omega L_{M0}) \end{bmatrix}, \qquad (48)$$

and therefore

$$X_{c,2} + X_{c,3} = \frac{CX_{c,1}(0)}{\det(A_C(s))} \cdot \left((s + j\omega^*_e)(L_{R0} - L_{M0}) + R_R - jn_p\omega(L_{R0} - L_{M0})\right). \qquad (49)$$

Generally, two of the three roots of $\det(A_C(s))$ are stable. Depending on whether the third root of $\det(A_C(s))=0$ is stable,

unstable, or zero, the time function $i_M(t)$ decays, grows, or converges to a steady-state as shown in Fig. 2. When there is a root at $s=0$, $\det\left(A_c(s)\right)$ can be factored as

$$\det(A_C(s)) = sp(s) \tag{50}$$

and the final value theorem allows us to conclude that the steady-state value is given by

$$\lim_{t\to\infty}\left(X_{c,2}(t)+X_{c,3}(t)\right)=\lim_{s\to 0}\left[s\frac{CX_{c,1}(0)}{\det(A_C(s))}\cdot\right.$$
$$\left.\left((s+j\omega_e^*)(L_{R0}-L_{M0})+R_R-jn_p\omega(L_{R0}-L_{M0})\right)\right] \tag{51}$$
$$=\frac{CX_{c,1}(0)}{p(0)}\left(R_R+\left(j\omega_e^*-jn_p\omega\right)\left(L_{R0}-L_{M0}\right)\right).$$

The denominator $p(0)$ can be determined from

$$p(0)=\left[\frac{d}{ds}(\det(A_C(s))\right]_{s=0} \tag{52}$$
$$=(-3a_0\omega_e^{*2}+2\omega_e^* n_p\omega a_0+a_2)+j(2a_1\omega_e^*-n_p\omega a_3),$$

where

$$a_0=C(L_{S0}L_{R0}-L_{M0}^2),$$
$$a_1=Y_L(L_{S0}L_{R0}-L_{M0}^2)+C(L_{S0}R_R+L_{R0}R_S),$$
$$a_2=Y_L(L_{S0}R_R+L_{R0}R_S)+CR_SR_R+L_{R0},$$
$$a_3=Y_L(L_{S0}L_{R0}-L_{M0}^2)+CR_SL_{R0}.$$

As a result, the steady-state value of the magnetizing current is

$$\lim_{t\to\infty} i_M(t)=\frac{CU_c}{|p(0)|}\left|R_R+\left(j\omega_e^*-jn_p\omega\right)\left(L_{R0}-L_{M0}\right)\right|, \tag{53}$$

and the value of the capacitor voltage needed to reach a magnetizing current equal to i_M^{*+} is

$$U_C=\frac{i_M^{*+}}{C}\sqrt{\frac{(-3a_0\omega_e^{*2}+2\omega_e^* n_p\omega a_0+a_2)^2+(2a_1\omega_e^*-n_p\omega a_3)^2}{R_R^2+(\omega_e^*-n_p\omega)^2(L_{R0}-L_{M0})^2}}. \tag{54}$$

This is the capacitor voltage needed to trigger self-excitation. Although the result was obtained using several approximations of questionable validity, (54) gives a value that can easily be computed, is remarkably accurate in practice, and shows the impact of various parameters on the capacitor voltage needed to trigger self-excitation.

III. Experimental Results

A. Operating Modes

Experimental results were obtained for a small two-phase induction motor (Bodine KCI-22A1, with rated values 7.5W, 24V, 60 Hz, and 3350 rpm). The parameters and analytical approximations of $L_M=f(i_M)$ and $L=f(i_M)$ were determined in [15] and are summarized in Appendix. The induction motor was tested as a generator by coupling it to a DC motor/tachometer under closed-loop velocity control. A DS1104 data acquisition and control board from dSPACE was used to implement the PID control law for the DC motor and to collect the data.

Fig. 3 shows the frequency of generation $f=\omega_e^*/2\pi$ as a function of capacitance for different speeds, as well as for different loading conditions, all obtained using the theoretical analysis and compared to experimental data. The computed steady-state voltage amplitude as a function of the capacitance and velocity was also found to be in good agreement with experimental results. When two values of i_M^* were possible, the one corresponding to the descending part of the magnetizing curve was used for computation.

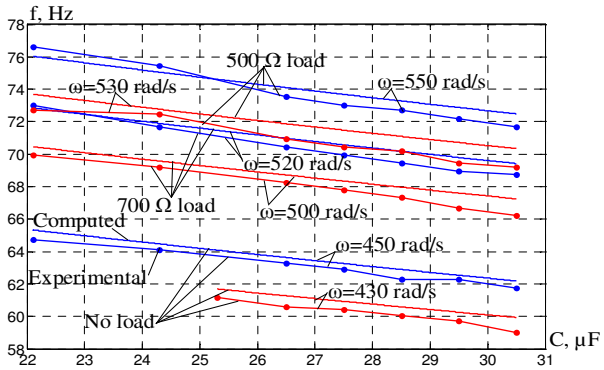

Fig. 3. Steady-state frequency as a function of capacitance for different velocities and loading conditions.

B. Stability of Operating Modes

The eigenvalues of the matrix A^* in (36) (with the specific choice of (40)) were computed in the velocity range from 424.5 rad/s to 925.1 rad/s, where L_M^* did not exceed L_{MAX}, and for the unloaded generator with 30.5 μF capacitor. The 6 eigenvalues always had the following characteristics: four were a pair of complex conjugates with negative real parts, one had a non-zero real value and one had a zero value. The zero eigenvalue is associated with the infinite number of equilibrium states and does not affect stability in a substantial way: there is no mechanism to lock the phase of the voltages and currents to an arbitrary time reference as in a grid-connected generator. A drift in phase also does not cause any problem. It was found that the complex eigenvalues did not change greatly with velocity, and were well into the stable side of the plane. The main factor influencing the stability was therefore the real eigenvalue (referred to as #5), which was closer to the imaginary axis.

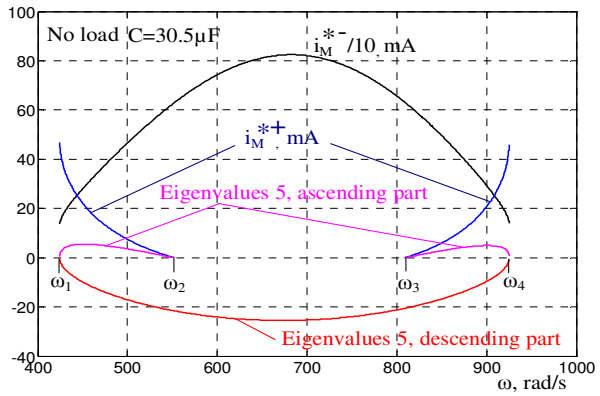

Fig. 4. Eigenvalue 5 and magnetizing current as function of velocity for the descending and the ascending parts of the magnetizing inductance curve.

Fig. 4 shows the possible solutions i_M^* and their associated eigenvalue 5 over a range of speeds. One finds that eigenvalue 5 is stable for i_M^{*-} (descending part) and for all velocities. Eigenvalue 5 for the ascending part only exists in a smaller range and is always unstable. Overall, one finds that there are five speed regions with boundaries labeled ω_1, ω_2, ω_3, and ω_4. Referring to the discussion of section II.D, the velocity ranges correspond to the following cases:

- $\omega < \omega_1$ and $\omega > \omega_4$ correspond to case 1: there is no stable steady-state magnetizing current other than zero.
- $\omega_1 < \omega < \omega_2$ and $\omega_3 < \omega < \omega_4$ correspond to case 2: there is a large stable magnetizing current, but also a smaller unstable magnetizing current. Self-excitation must be triggered to reach a magnetizing current greater than or equal to i_M^{*+}.
- $\omega_2 < \omega < \omega_3$ corresponds to case 3: there is a single stable magnetizing current. Spontaneous self-excitation will occur in this range due to small initial conditions such as residual flux.

Note that the speed range of Fig.4 extends well beyond the rated speed of the motor. Operating limits may restrict generation to the leftmost side of the range. For some values of capacitance and load, cases were found where the velocity range from ω_2 to ω_3 did not exist. In such cases, only triggered self-excitation is possible.

C. *Boundaries of Self-Excitation*

The boundaries of self-excitation were computed for the generator with no load, 700Ω, and 500Ω loads using the procedure of section II.E with $L_M^* = L_{MAX}$. The experimental validation of these boundaries was performed by determining *collapse* regions. Specifically, the generator was spun at a high velocity and an initial voltage was applied to the capacitor in one of the phases, triggering self-excitation. Then, the velocity was reduced until the voltage collapsed. The result defined the experimental boundary for self-excitation. The results are plotted in Fig. 5, which shows good agreement between the self-excitation boundaries and the experimental collapse boundaries.

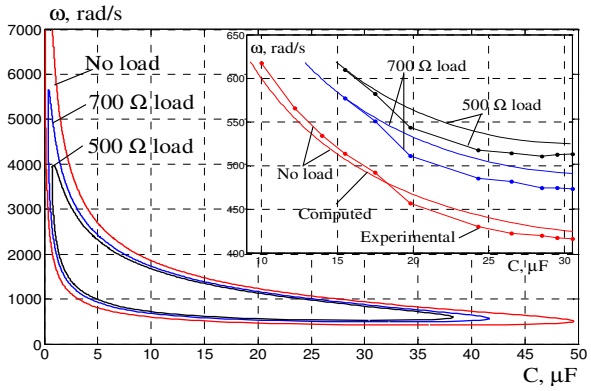

Fig. 5. Self-excitation boundaries.

Spontaneous self-excitation was experimentally observed in the velocity range from 620 to 670 rad/s for capacitors 30.5, 22.1 and 15μF and no load. Triggered self-excitation was observed at much lower speeds, closer to the normal operating speed of the motor. In the experiments of triggered self-excitation, various values of capacitors were tested by placing capacitors in parallel. For practical reasons, only one of the capacitors in one of the windings, C_1 with a value of 10μF, was pre-charged with some voltage U_{C1}. At the initial time, the capacitor was either connected to the winding, or connected in parallel with the other capacitors already connected to the winding. The charge associated with the voltage U_{C1} was immediately redistributed to all the capacitors of the winding, so that the equivalent voltage applied to the capacitors was $U_C = U_{C1}\, C_1/C$, where C was the total capacitor value of each phase.

Fig. 6 shows the experimental boundaries for triggered self-excitation with different U_{C1} and loads. The computed boundaries for self-excitation and spontaneous self-excitation are shown on the same graph. Generally, one would expect that the triggered self-excitation boundaries would be delimited by the boundary of spontaneous self-excitation (associated with a zero voltage, which means no triggering) and the general self-excitation boundary (associated with the value of U_{C1} needed to produce the magnetizing current corresponding to L_{MAX}). The data is consistent with this assumption (curves 2 to 5 are between curves 1 and 6, and curves 8 to 10 are between curves 7 and 11).

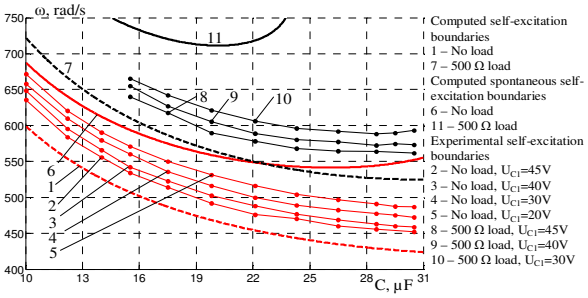

Fig. 6. Computed and experimental self-excitation boundaries.

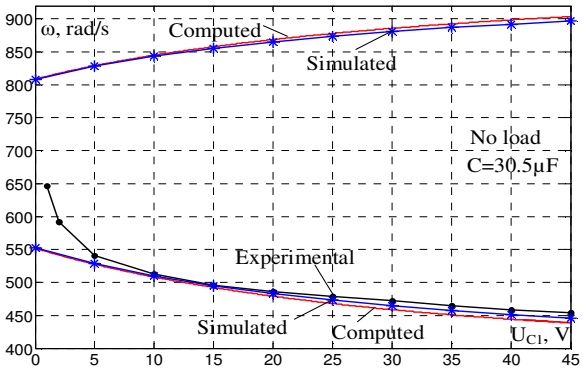

Fig. 7. Velocity needed to trigger self-excitation as a function of the initial capacitor voltage U_{C1}.

Fig. 7 shows the remarkable accuracy of the simple formula (54) in predicting the success of a given voltage in triggering self-excitation. The case with no load and C=30.5 μF was considered. The figure shows the velocity needed to trigger self-excitation as a function of the voltage U_{C1} applied to the capacitor C_1. As may be expected, increases of U_{C1} lead to a decrease in the minimum velocity necessary to trigger self-excitation. The computed curve based on equation (54) is close to the experimental one, except in the low voltage range. This part of the plot is associated with the nonlinearity of the magnetizing inductance at very low current. It is possible that the difficulty in measuring this part of the characteristic is the source of the error, although other causes are not excluded.

The plot also shows the speeds that were needed in simulations using the dynamic model. It was found that substitution of L_M^*, L_S^* and L_R^* corresponding to i_M^{*+} into equations (52)-(54) (instead of L_{M0}, L_{S0} and L_{R0}) made the simulation and computational results match better. Simulations show that the prediction of the analytical formula is accurate for the lower curve of the speed range as well as the higher curve, where mechanical constraints did not permit experiments.

D. Transient Responses Close to the Boundary

Interesting transient responses are observed for initial conditions close to the self-excitation boundary. The voltage built-up caused by triggering is shown in Fig. 8. The velocity is slightly greater than the minimum for self-excitation specified by Figs. 6 or 7. The synchronous frequency is 72 Hz and the frequency of the voltage is 62 Hz.

In Fig. 8, a temporary steady-state is visible for about 0.2 s. The magnetizing inductance and the log of the magnitude of the voltage vector are shown as subplots of Fig. 8. If divergence from the unstable equilibrium state was exponential, the growth of the log plot would be linear. This is clearly not the case, but when L_M reaches L_{MAX}, the logarithmic curve of the RMS phase voltage has a linear part (from about 0.7 to 1 s).

The subplot for the log of the voltage also shows the result of the simulation, which is in very good agreement with the experiment. It was found that, when the operating conditions were farther from the triggered self-excitation border, the voltage build-up occurred faster and the initial growth of the log of the voltage was close to linear.

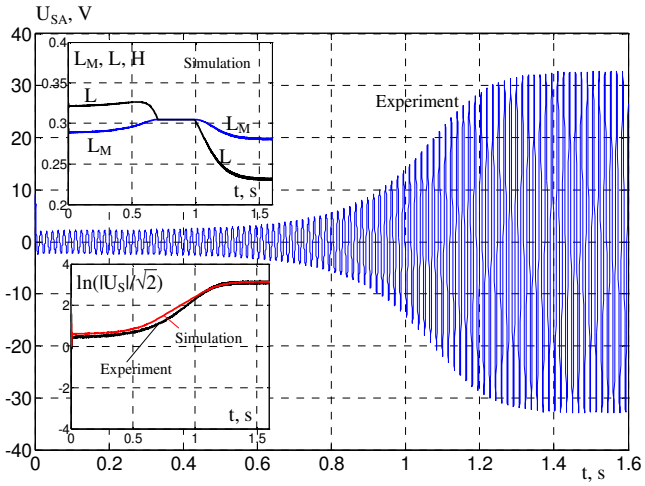

Fig. 8. The process of voltage built-up of the unloaded generator with 452 rad/s velocity, 30.5 μF capacitors and U_{C1}=45 V.

Fig. 9 shows the result of an experiment where the speed was 450 rad/s, slightly below the triggered self-excitation border. The initial capacitor charge was sufficient to trigger a generating condition lasting for many cycles, followed by a voltage collapse. Experiments have also shown that if the velocity was lower than 450 rad/s, the voltage collapse occurred faster.

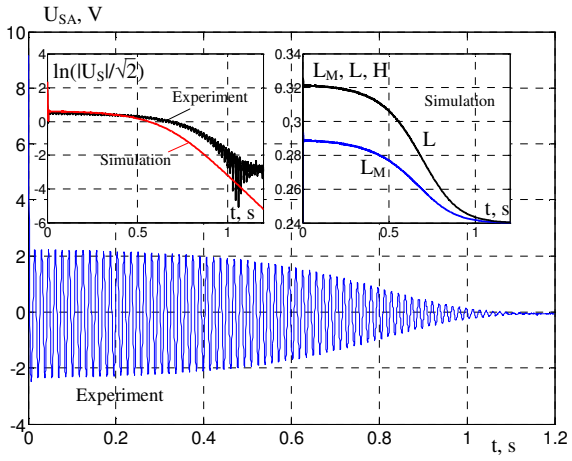

Fig. 9. The process of the unsuccessful voltage built-up of the unloaded generator with 450 rad/s velocity, 30.5 μF capacitors and U_{C1}=45 V.

The simulation shown in the subplot of Fig. 9 for the log of the voltage is not as close as in the previous plot, but correctly predicts the voltage collapse. It was also found that, if the velocity remained 452 rad/s but the initial voltage dropped from 45V to 40V, voltage collapse would also result. So, not only a tiny difference in velocity, but also a small change in initial capacitor voltage can make the difference between a sustained, power generating mode, and a useless steady-state with zero voltages and currents.

In practice, triggered self-excitation requires an additional circuit and a battery to pre-charge the capacitors. The benefit is that self-excitation can be started from lower velocities. If

the speed of the generator is reduced after self-excitation, power production will continue until the general boundary of self-excitation is reached (regardless of how self-excitation was obtained originally). If, however, the speed is so reduced that voltages collapse, self-excitation can again be restarted for a lower speed with triggered self-excitation than with spontaneous self-excitation.

IV. EXTENSIONS

A. *Resistive/inductive loads*

For loads modeled as a resistive component with admittance Y_L connected in series with an inductance L_L, the state-space model is obtained by replacing equation (2) by

$$\begin{aligned} -C\frac{dU_S}{dt} &= i_S + i_L + \omega_e C J U_S \\ Y_L L_L \frac{di_L}{dt} &= Y_L U_S - i_L - \omega_e Y_L L_L J i_L \end{aligned}, \qquad (55)$$

where i_L is the current flowing in the load. This extension adds two differential equations defining i_L to the state-space model.

While the analysis of the paper would need to be extended to consider such case, preliminary simulations show that similar properties hold for the resistive/inductive case. Fig. 10 shows the relationship between the speed of the generator and the capacitor voltage needed to trigger self-excitation. The figure shows the simulation results for the purely resistive load (with the experimental results presented earlier), as well as two cases of resistive/inductive loads. One sees that the trends are similar in all cases although, perhaps surprisingly, an increase in load inductance reduces the speed needed to trigger self-excitation.

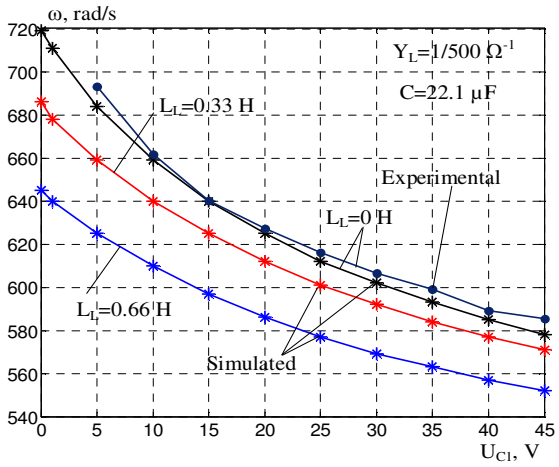

Fig. 10. Velocity needed to trigger self-excitation as a function of the initial capacitor voltage U_{C1} in the case of a resistive/inductive load.

B. *Model of core losses*

An approximate model of core losses consists of a resistance connected in parallel with the magnetizing inductance [20]. Assuming such a model and a resistance R_{Fe} with a current i_{Fe} flowing in the resistance, equations (4) and (5) are replaced by

$$i_M = \sqrt{{i_{MF}}^2 + {i_{MG}}^2}\,, \; i_{MF} = i_{SF} + i_{RF} + i_{FeF}\,,$$

$$\begin{aligned} i_{MG} &= i_{SG} + i_{RG} + i_{FeG}\,, \\ \Psi_S &= L_{\sigma S} i_S + L_M (i_S + i_R + i_{Fe})\,, \\ \Psi_R &= L_{\sigma R} i_R + L_M (i_S + i_R + i_{Fe})\,, \end{aligned} \qquad (56)$$

while (11) becomes

$$\begin{aligned} \frac{d\Psi_S}{dt} &= (L_{\sigma S} + L_M)\frac{di_S}{dt} + L_M\frac{di_R}{dt} + L_M\frac{di_{Fe}}{dt} + \frac{dL_M}{dt}(i_S + i_R + i_{Fe})\,, \\ \frac{d\Psi_R}{dt} &= (L_{\sigma R} + L_M)\frac{di_R}{dt} + L_M\frac{di_S}{dt} + L_M\frac{di_{Fe}}{dt} + \frac{dL_M}{dt}(i_S + i_R + i_{Fe}). \end{aligned} \qquad (57)$$

A new equation is also added

$$\begin{aligned} &L_M\frac{di_R}{dt} + L_M\frac{di_S}{dt} + L_M\frac{di_{Fe}}{dt} + \frac{dL_M}{dt}(i_S + i_R + i_{Fe}) \\ &\quad = -R_{Fe} i_{Fe} - \omega_e J L_M (i_S + i_R + i_{Fe}). \end{aligned} \qquad (58)$$

This extension adds two differential equations defining i_{Fe} to the state-space model.

C. *Sudden changes of load*

The state-space model and the analysis make it possible to consider cases where the load suddenly increases during self-excitation. Fig. 11 shows the results of simulations where the generator self-excites with no load. The magnetizing current is shown for the no-load case as well as for two simulations where the load suddenly increases before self-excitation has reached the steady-state. The initial magnetizing current, triggered by a capacitor voltage, is greater than the no-load requirement, but smaller than for the loaded generator. The difference between the two additional curves is in the timing of the load increase. In the first case, the magnetizing current has not reached the value required by the higher load, while it has reached the minimum value in the second case. The difference of timing is tiny (0.34s *vs.* 0.37s), but makes the difference between sustained self-excitation and voltage collapse.

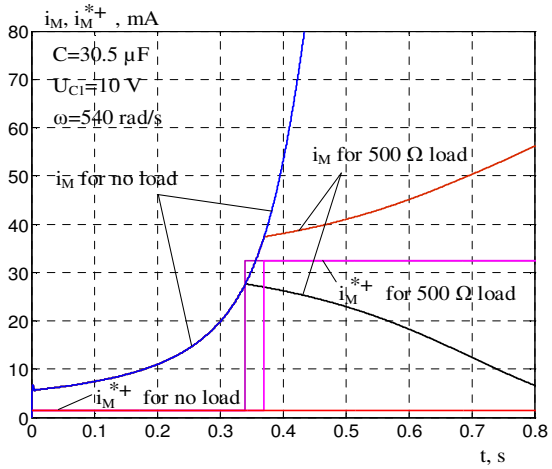

Fig. 11. Magnetizing current built-up during sudden load change.

D. *Applications to larger machines*

Although the experiments of this paper were performed with a small induction machine, the principles are applicable to large machines as well. To illustrate this point, computations and simulations were performed for a three-phase generator model

adapted from [14]. The rated values were 415V, 7.8A, 3.6 kW, 50 Hz, and the parameters were R_S=1.7Ω, R_R=2.7Ω, $L_{\sigma S}$=$L_{\sigma R}$=0.0114H, n_p=2, L_{MAX}=0.295H, L_{M0}=0.23H, i_{M1}=0.893A.

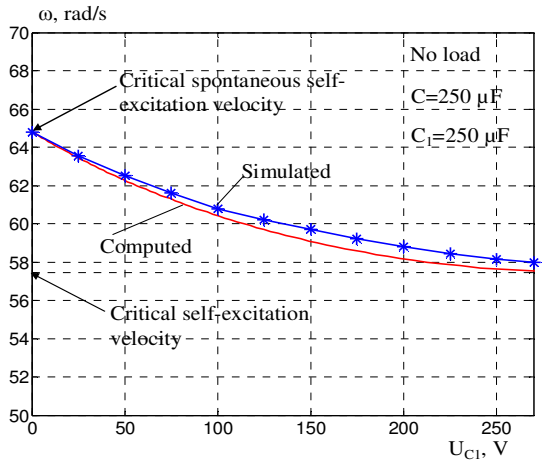

Fig. 12. Velocity needed to trigger self-excitation as a function of the initial capacitor voltage U_{C1} for a larger machine.

Fig. 12 shows the relationship between the capacitor voltage needed to trigger self-excitation and the speed of the generator. The trend is similar to the trend observed with the smaller generator, and the match between the computed and simulated data is comparable. However, the benefit of triggered self-excitation in terms of speed is smaller than for the original generator.

V. Conclusions

The paper proposed a nonlinear dynamic model for an induction generator connected to resistive loads and capacitors. Using the model, it was found that the induction generator could have a single zero equilibrium steady-state or, in addition, a stable nonzero steady-state, or two steady-states with one stable and one unstable. The operating velocity range was thus found to be divided into three types. The first one is such that self-excitation is not possible. The second is such that self-excitation is spontaneous, meaning that arbitrarily small initial conditions can trigger self-excitation. The third is such that self-excitation is possible, but needs to be triggered by reaching a magnetizing current greater than or equal to the current associated with the unstable steady-state. A by-product of the analysis is a formula that computes explicitly the voltage needed to trigger self-excitation. Very good agreement was observed between the computational, simulated, and experimental results. By careful choice of initial conditions, sustained periods of self-excitation were found possible, leading to either voltage growth and power production, or voltage collapse. The results unify and extend previous theories of self-excitation, in addition to providing new insights into its mechanisms.

Appendix: Analytic Approximation of Magnetizing Inductance Curve

To facilitate numerical computations, an analytic approximation of the magnetizing curve obtained experimentally was used. The approximation of the magnetizing inductance curve was developed in [15] and verified experimentally. Three regions are defined, with breakpoints i_{M1} and i_{M2}:

- for $i_M<i_{M1}$ (the ascending part): the instantaneous magnetizing inductance is approximated by
$$L_M = L_{MAX} - b_1(i_M - i_{M1})^2, \quad (59)$$
where b_1 is a coefficient to be adjusted. In this region, the dynamic magnetizing inductance is
$$L = L_{MAX} - b_1 i_{M1}^2 - b_1 i_M (3i_M - 4i_{M1}). \quad (60)$$
- for $i_{M1}<i_M<i_{M2}$ (the flat part): both magnetizing inductances are constant with L=L_M=L_{MAX}. If the value L_{M0} is picked for i_M=0, the coefficient b_1 in the first region must be taken as
$$b_1 = (L_{MAX} - L_{M0})/i_{M1}^2. \quad (61)$$
- for $i_M > i_{M2}$ (the descending part): the magnetizing inductances are approximated by
$$L_M = (\Psi_{M3} + \sqrt{(i_M - i_{M3})/b_3})/i_M, \quad (62)$$
$$L = 1/\sqrt{4b_3(i_M - i_{M3})}, \quad (63)$$
where b_3 is a coefficient to be adjusted so that
$$i_{M3} = i_{M2} - 1/(4b_3 L_{MAX}^2), \quad (64)$$
$$\Psi_{M3} = L_{MAX} i_{M2} - \sqrt{(i_{M2} - i_{M3})/b_3}, \quad (65)$$
(in this manner, for i_M=i_{M2}, L_M=L=L_{MAX}).

Overall, the parameters of the model of the generator were estimated to be R_S=49.5Ω, R_R=24Ω, $L_{\sigma S}$=$L_{\sigma R}$=0.027H, n_p=1, L_{MAX}=0.305H, L_{M0}=0.24H, b_3=11A/Wb^2, i_{M1}=0.0477A, i_{M2}=0.134A.

References

[1] S.S. Murthy, O.P. Malik, & A.K. Tandon, "Analysis of self-excited induction generators," *IEE Proc.,* vol. 129, pt. C, no. 6, 1982, pp. 260-265.

[2] S.S. Murthy, B. Singh, & A.K.Tandon, "Dynamic models for the transient analysis of induction machines with asymmetrical connection," *Electr. Mach. and Electromech.*, 1981, no. 6, pp. 479-492.

[3] N.H. Malik & A.K. Al-Bahrani, "Influence of the terminal capacitor on the performance characteristics of a self excited induction generator," *IEE Proc.*, vol. 137, no. 2, 1990, pp. 168-173.

[4] A.K. Tandon, S.S.Murthy, & G.J.Berg, "Steady-state analysis of capacitor self-excited induction generators," *IEEE Trans. Power Apparatus and Systems*, vol. 103, no. 3, 1984, pp. 612-618.

[5] L. Ouazene & G. McPherson Jr., "Analysis of the isolated induction generator," *IEEE Trans. Power Apparatus and Systems*, vol. 102, no. 8, 1983, pp. 2793-2798.

[6] J.M. Elder, J.T. Boys & J.L. Woodward, "Self-excited induction machine as a small low-cost generator," *IEE Proc*., Pt. C, vol. 131, no. 2, 1984, pp. 33-41.

[7] S.M. Alghuwainem, "Steady-state analysis of an isolated self-excited induction generator driven by regulated and unregulated turbine," *IEEE Trans. Energy Conversion,* vol. 14, no. 3, 1999, pp. 718-723.

[8] C. Grantham, D. Sutanto, & B. Mismail, "Steady-state and transient analysis of self-excited induction generators," *IEE Proc.,* vol. 136, pt. B, no. 2, 1989, pp. 61-68.

[9] T.F. Chan, "Capacitance requirements of self-excited induction generators," *IEEE Trans. Energy Conversion*, vol. 8, no. 2, 1993, pp. 304-311.

[10] O. Ojo, "Minimum airgap flux linkage requirement for self-excitation in stand-alone induction generators," *IEEE Trans. Energy Conversion*, vol. 10, no. 3, 1995, pp. 484-492.

[11] S.-C. Kuo & L. Wang, "Dynamic eigenvalue analysis of a self-excited induction generator feeding an induction motor," *Winter Meeting of the IEEE Power Engineering Society*, vol. 3, 2001, pp. 1393 - 1397.
[12] M. Bodson & O. Kiselychnyk, "Analytic conditions for spontaneous self-excitation in induction generators," *Proc. of the American Control Conference*, Baltimore, MD, pp. 2527-2532, 2010.
[13] J.M. Elder, J.T. Boys, & J.L.Woodward, "The process of self excitation in induction generators," *IEE Proc.,* vol. 130, pt. B, no. 2, 1983, pp.103-108.
[14] D. Seyoum, C. Grantham, & F. Rahman, "The dynamic characteristics of an isolated self-excited induction generator driven by a wind turbine," *IEEE Trans. Industry Applications,* vol. 39, no. 4, 2003, pp. 936-944.
[15] M. Bodson & O. Kiselychnyk, "On the triggering of self-excitation in induction generators," *Proc. of the 20th International Symposium on Power Electronics, Electrical Drives, Automation and Motion (Speedam 2010)*, Pisa, Italy, pp. 866-871, 2010.
[16] E. Levi, "A unified approach to main flux saturation modeling in d-q axis models of induction machines," *IEEE Trans. Energy Conversion,* vol. 10, no. 3, 1995, pp. 455-461.
[17] E. Levi, "Main flux saturation modeling in double-cage and deep-bar induction machines," *IEEE Trans. Energy Conversion,* vol. 11, no. 2, 1996, pp. 305-311.
[18] M. Bodson & O. Kiselychnyk, "Nonlinear dynamic model and stability analysis of self-excited induction generators," *Proc. of the American Control Conference*, San Francisco, CA, pp. 4574-4579, 2011.
[19] M. Bodson & O. Kiselychnyk, "On the capacitor voltage needed to trigger self-excitation in induction generators," *Proc. of 19-th Mediterranean Conference on Control and Automation*, Corfu, Greece, pp. 351-357, 2011.
[20] I. Boldea, Variable speed generators, CRC Press, Boca Raton, FL, 2006.

Marc Bodson received a Ph.D. degree in Electrical Engineering and Computer Science from the University of California, Berkeley, in 1986. He obtained two M.S. degrees - one in Electrical Engineering and Computer Science and the other in Aeronautics and Astronautics - from the Massachusetts Institute of Technology, Cambridge MA, in 1982. Currently, Marc Bodson is a Professor of Electrical & Computer Engineering at the University of Utah in Salt Lake City. He was Chair of the Department of Electrical & Computer Engineering between July 2003 and October 2009, and he was the Editor-in-Chief of *IEEE Trans. on Control Systems Technology* between January 2000 and December 2003. He was elected Fellow of the Institute of Electrical and Electronics Engineers in 2006. His research interests are in adaptive control, with applications to electromechanical systems and aerospace.

Oleh Kiselychnyk was born in Truskavets, Ukraine, in 1970. He received the M.Sc. and Ph.D. degrees in Electrical Engineering and Automation from the National Technical University of Ukraine "Kiev Polytechnic Institute" (NTUU "KPI") in 1993 and 1997 respectively. Currently, he is an Associate Professor in the department of automation of electromechanical systems and electric drives of NTUU "KPI". He was a Visiting Fulbright Scholar at the University of Utah, USA, in 2009 and a Visiting Researcher at the Hamburg University of Technology, Germany, 2008. His main research interests are control of electric motors and generators, automation of water supply systems, and microcontrollers.